Energetics of numerical geodynamo models

B. A. Buffett[1] and J. Bloxham[2]

[1]*Department of Earth and Ocean Sciences, University of British Columbia, Vancouver,* BC V6T 1Z4, *Canada*
[2]*Department of Earth and Planetary Sciences, Harvard University, Cambridge,* MA 02138, *USA*

SUMMARY

Global energy balances provide a useful framework for assessing the operation of numerical geodynamo models. We apply a spectral decomposition to the magnetic and kinetic energy equations to assess how the magnetic field is regenerated by convection in these models. Specific analysis of the Kuang and Bloxham model indicates that dynamo action relies on the combined effects of buoyant upwelling and shear in the zonal flow. The part of the flow that contributes most to the generation of the dipole field is associated with a narrow range of local magnetic Reynolds number around $R_m \approx \mathcal{O}(1)$. Shear in the zonal flow converts the dipole field into a strong toroidal field. The equilibration of field generation is revealed in the time-dependent exchanges of kinetic and magnetic energies. We also assess the turbulent cascade of energy to small scales. Transfer of kinetic energy to small scales is represented by a turbulent viscosity, which varies substantially with the length scale of the motion. This result implies that models for turbulent viscosity should depend on the wavenumber of the motion.

Key words: convection, dynamo theory, Earth's core, geomagnetism.

1 INTRODUCTION

The geomagnetic field is sustained by fluid motion in the Earth's liquid iron core. Convection is the most likely cause of the fluid motion, though many aspects of the process are poorly understood. Important advances in recent years have been achieved using numerical models of convection-driven dynamos in spherical shells (Jones *et al.* 1995; Glatzmaier & Roberts 1995, 1996; Kuang & Bloxham 1997; Busse *et al.* 1998; Kageyama & Sato 1998; Olson *et al.* 1999). Many of these calculations predict dipole fields that are comparable in strength to the Earth's field. Even the non-dipole part of the predicted field exhibits similarities with the observed field (Kuang & Bloxham 1997; Christensen *et al.* 1998). However, comparisons with the field at the Earth's surface are not sufficient to elicit internal details about the generation mechanisms.

Comparison of recent geodynamo models reveals that different styles of field generation are possible. These differences are attributed to the choice of parameter values or the assumptions used in the numerical calculation. For example, some studies favour the use of stress-free boundary conditions to minimize the effects of viscosity (Kuang & Bloxham 1997), whereas others have attempted to reduce the effects of inertia to Earth-like values (Glatzmaier & Roberts 1996). All models are still very far from realistic simulations of the geodynamo, so approximations of one form or another are inevitable. However, it is not presently clear how conditions in the core are best approximated. In some instances it has been possible to demonstrate explicitly the effect of different assumptions on the operation of the geodynamo (Kuang & Bloxham 1997), although the underlying cause of changes in the solution are not well under-

stood. Without a good physical understanding of the changes in the solution, it is difficult to appraise different modelling strategies.

Systematic surveys of the accessible range of parameter values have begun to categorize different style of dynamo action (Christensen *et al.* 1999; Grote *et al.* 2000a). The diagnostics used to distinguish these results typically include the relative strength of the dipole field or the time-averaged spectra of kinetic and magnetic energies. While these diagnostics are useful for distinguishing numerical models, they do not reveal the origin of the differences. More detailed investigations of the internal dynamics have focused on the force balance (Kuang 1999) and the energy balance (Olson *et al.* 1999) in the core. The study of Kuang (1999) was primarily concerned with the role of viscous stresses near the core–mantle boundary, whereas Olson *et al.* (1999) examined the spatial correlation between the buoyancy flux and ohmic dissipation in assessing the mechanisms responsible for equilibrating the generation of the magnetic field.

Analysis of the energetics of the geodynamo models provides a powerful means of probing the internal dynamics of these models. Global energy balances can be used to assess the rate at which energy is supplied to the geodynamo by a flux of heat and light elements at the boundaries. Quantifying the conversion of this energy supply to kinetic and magnetic energies characterizes the style of convection and dynamo action. Viscous and ohmic dissipation ultimately convert the input energy to heat. More detailed insights emerge from a spectral decomposition of the energy balances. Conversion of energy from one form to another can be tracked over all spatial scales in the calculation as a function of time. We can identify the parts of the flow that sustain the dipole field or assess the cascade of kinetic

and magnetic energies to small scales. Time averages are particularly helpful in identifying the existence of mean states, whereas fluctuations about the mean state are important for characterizing instabilities that lead to phenomena such as magnetic reversals.

Here we assess the energetics of geodynamo simulations using the Kuang–Bloxham model (Kuang & Bloxham 1997, 1999). We describe the global balances for magnetic and kinetic energy, and derive general expressions for the spectral decomposition of these energy balances. Temporal and spatial variations in the energy balances reveal a surprisingly simple behaviour. To a first approximation the gravitational energy released by buoyant fluid at most spatial scales in the model is balanced by ohmic and viscous losses at the same scales. Small imbalances are the result of energy transfers between different spatial scales. We show that transfers of energy between scales are crucial for the operation of the geodynamo. We focus specifically on the transfer of energy to the dipole field from smaller scale motions. We also examine the cascade of energy from large scales to small with the aim of assessing the scale dependence of turbulent diffusivities.

2 GLOBAL ENERGY BALANCES

Global balances for the kinetic and magnetic energy in the core are obtained by integrating over the volume of the core the equations for magnetic induction and local momentum conservation (e.g. Backus 1975; Hewitt *et al.* 1975). These global energy balances are well known, so the goal of this section is to ensure consistency between the form of the energy balances and the approximations used in the geodynamo model. We summarize the main results below and defer the spectral decomposition to the next section.

2.1 Dimensional equations

The global energy balances are derived from the local equations for magnetic induction and momentum conservation. The induction equation is obtained from Maxwell's equations for a moving conductor under the usual assumption that the velocity $\mathbf{v}$ of the conductor is small compared with the speed of light (e.g. Braginsky & Roberts 1995). The electrical conductivity σ of the conductor is assumed to be constant and the magnetic permeability is assumed to have the value of free space. An electric current density $\mathbf{J}$ in the conductor produces the magnetic field $\mathbf{B}$ and causes a Lorentz force $\mathbf{L}$ on the material.

The model of Kuang and Bloxham uses a Boussinesq approximation of the local momentum equation. The motion of a fluid with constant density ρ is described in a frame of reference that rotates with constant angular velocity Ω. Convection is driven by thermal buoyancy which results from an imposed temperature gradient h at the inner radius of the shell. The resulting variation in density is defined by

$$\Delta\rho = -\rho\alpha\Theta \tag{1}$$

where α is the coefficient of thermal expansion and Θ is the deviation from a purely conductive temperature profile $T_0(r)$. All of the model calculations used in this study assume that the boundaries of the outer core are impermeable and undeformable. Viscous stress-free boundary conditions are also imposed in the calculations.

We express the global energy balances as integrals over the volume of the liquid outer core, which we denote by V and let $\mathbf{dS}$ be the outward surface normal. With the preceding assumptions, the global magnetic energy equation can be expressed in the form (Bullard & Gellman 1954)

$$\int_V \frac{\partial}{\partial t}\left(\frac{\mathbf{B}^2}{2\mu}\right) dV = \frac{1}{\mu}\int_V \mathbf{B}\cdot\nabla\times(\mathbf{v}\times\mathbf{B})\,dV - \int_V \frac{J^2}{\sigma}\,dV$$
$$- \int_S \eta(\mathbf{J}\times\mathbf{B})\cdot\mathbf{dS} \tag{2}$$

where $\eta = 1/\sigma\mu$ is the magnetic diffusivity. The surface integral in (2) can be rearranged using the identity $\mathbf{J}\times\mathbf{B}/\sigma = \mathbf{E}\times\mathbf{B}$, though the form given in (2) is more convenient for our purposes. The global equation for kinetic energy is

$$\int_V \frac{\partial}{\partial t}\left(\frac{\rho\mathbf{v}^2}{2}\right) dV = \int_V \mathbf{v}\cdot\mathbf{L}\,dV - \int_V \rho\alpha\Theta\mathbf{v}\cdot\mathbf{g}\,dV$$
$$- \int_V 2\rho\nu\dot{\mathbf{e}}^2\,dV \tag{3}$$

where the gravitational acceleration $\mathbf{g}$ is a linear function of radius r in the constant density fluid and the strain-rate tensor $\dot{\mathbf{e}}$ is related to the fluid velocity by Landau & Lifshitz (1987)

$$\dot{\mathbf{e}} = \frac{1}{2}[\nabla\mathbf{v} + (\nabla\mathbf{v})^T]. \tag{4}$$

2.2 Non-dimensional equations

Kuang & Bloxham (1999) express the governing equations in non-dimensional form using the outer radius r_o of the core as the length scale. The magnetic diffusion time r_0^2/η is the timescale and the temperature scale is hr_o. The magnetic field is scaled by $\mathcal{B} = (2\Omega\rho\mu\eta)^{1/2}$ and the electric current is scaled by $\mathcal{B}/(\mu r_o)$. It follows that the non-dimensional energy is measured in terms of $2\Omega\rho\eta r_o^3$ and the rate of change of energy is scaled by $2\Omega\rho\eta^2 r_o$. The non-dimensional version of the magnetic energy equation in (2) becomes

$$\frac{1}{2}\int_V \frac{\partial\mathbf{B}^2}{\partial t}\,dV = \int_V \mathbf{B}\cdot\nabla\times(\mathbf{v}\times\mathbf{B})\,dV - \int_V H_\eta\mathbf{J}^2\,dV$$
$$- \int_S H_\eta(\mathbf{J}\times\mathbf{B})\cdot\mathbf{dS} \tag{5}$$

while the kinetic energy equation in (3) becomes

$$\frac{Ro}{2}\int_V \frac{\partial\mathbf{v}^2}{\partial t}\,dV = \int_V \mathbf{v}\cdot\mathbf{L}\,dV + Ra\int_V \Theta\mathbf{v}\cdot\mathbf{r}\,dV$$
$$- 2E\int_V H_\nu\dot{\mathbf{e}}^2\,dV \tag{6}$$

where

$$Ro = \frac{\eta}{2\Omega r_o^2} \tag{7}$$

is the magnetic Rossby number,

$$Ra = \frac{\alpha g(r_o)hr_o^2}{2\Omega\eta} \tag{8}$$

is the Rayleigh number,

$$E = \frac{\nu}{2\Omega r_o^2} \tag{9}$$

is the Ekman number. The terms H_η and H_ν are complicated operators that enhance magnetic diffusion and viscosity relative to the nominal values used in the definition of the timescale and E, respectively. Enhanced diffusion is normally applied as a scale-dependent diffusivity in the spectral domain, which means that the spatial representation has the form of a convolution integral. As a result, numerical evaluation of (5) and (6) using the geodynamo

model is performed most easily in the spectral domain. We defer the spectral decomposition of (5) and (6) to the next section and conclude by giving a brief physical interpretation of these global energy balances.

2.3 Interpretation

Eqs (5) and (6) identify the sources and sinks of magnetic and kinetic energy in the geodynamo. Dynamo action is described by the first volume integral on the right-hand side of (5), whereas the loss of magnetic energy occurs through ohmic dissipation in the interior of the liquid outer core and through the Poynting flux of energy across the boundaries of the outer core. Most of the magnetic energy flux from the outer core is converted to heat by ohmic losses in the inner core and the conducting part of the mantle. In the Kuang–Bloxham model, the conducting part of the mantle is confined to a thin layer at the base of the mantle, corresponding roughly to D''.

The kinetic energy equation in (6) indicates that kinetic energy is maintained by a radial flux of buoyant fluid through the outer core. This energy source defines the rate at which gravitational energy is released by cold downwelling and hot upwelling. Losses of kinetic energy result from viscous dissipation, whereas the work done by Lorentz forces can be either positive or negative. We expect the work done by Lorentz forces to be negative on average because it must account for the transfer of kinetic energy to magnetic energy through dynamo action.

In order to clarify the connection between the kinetic and magnetic energy equations, we re-express the source term for magnetic energy in the form

$$\int_V \mathbf{B} \cdot \nabla \times (\mathbf{v} \times \mathbf{B}) \, dV = \int_V \mathbf{B} \cdot (\dot{\mathbf{e}} \cdot \mathbf{B}) \, dV \tag{10}$$

where we make use of the boundary condition $\mathbf{v} \cdot \mathbf{dS} = 0$. The right-hand side may be interpreted as the rate at which the magnetic field is amplified by strain of the conducting fluid. For comparison, the work done by Lorentz forces can be manipulated into the form

$$\int_V \mathbf{v} \cdot \mathbf{L} \, dV = -\int_V \mathbf{B} \cdot (\dot{\mathbf{e}} \cdot \mathbf{B}) \, dV + \int_S \mathbf{v} \cdot \mathbf{M} \cdot \mathbf{dS} \tag{11}$$

where the Maxwell stress tensor $\mathbf{M}$ is defined (in dimensionless form) by

$$M_{ij} = B_i B_j - (1/2) B^2 \delta_{ij} \tag{12}$$

and δ_{ij} is the Kronecker delta. The magnetic source term in (10) appears in (11) with the opposite sign. This means that the energy supplied to the magnetic field is drawn from the kinetic energy. The surface integral in (11) represents the work done on the fluid core by Maxwell stresses at its boundaries. These stresses transfer kinetic energy (and angular momentum) between the fluid outer core and the surrounding solid inner core and mantle. Because the changes in the kinetic energy of the inner core and mantle vanish when averaged over a suitably long interval of time, we expect the work done by Maxwell stresses on the outer core to have no influence on the long-term energetics of the geodynamo.

Fig. 1 illustrates the time-averaged flow of energy through the geodynamo. Gravitational energy (in the form of buoyant fluid at the boundaries of the outer core) is converted to kinetic energy by convection. Some of this kinetic energy is converted to magnetic energy by dynamo action, while the rest is converted to heat by viscous friction. Magnetic energy is also converted to heat by ohmic losses. The volume integral of $\mathbf{J}^2$ in (5) accounts for ohmic losses in the interior the fluid outer core, whereas the surface integral (in
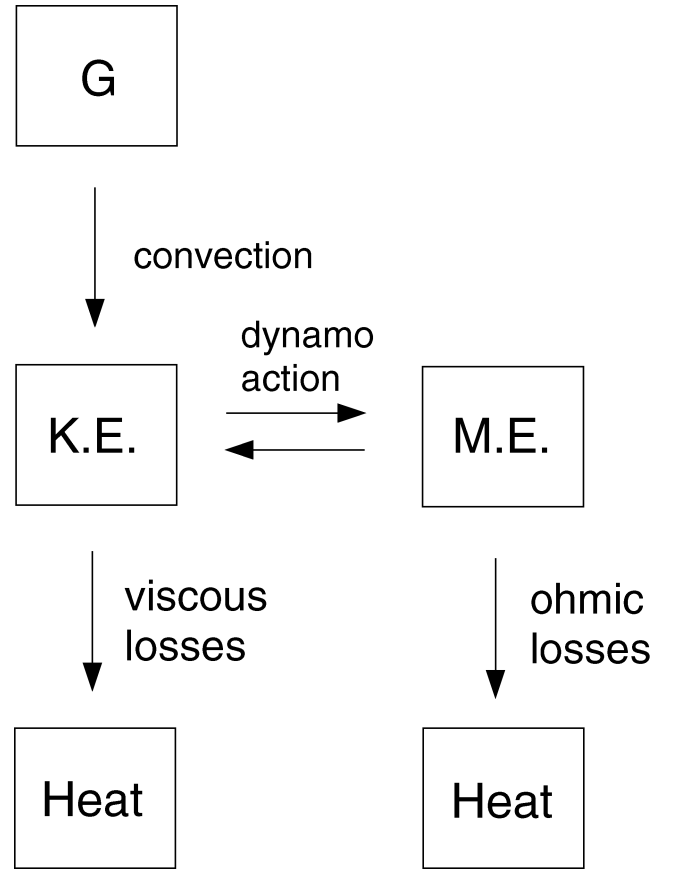
Figure 1. Schematic illustration of the time-averaged flow of energy through the geodynamo. Energy is supplied to the geodynamo by the release of gravitational energy *G* due to buoyant fluid at the boundaries. Convection converts the gravitational energy to kinetic energy (K.E.), which is transformed to magnetic energy (M.E.) by dynamo action. Viscous and ohmic losses convert K.E. and M.E. to heat.

the time-averaged equation) is equal to the ohmic losses that occur inside the solid inner core and conducting part of the mantle. We subsequently refer to these two terms collectively as the ohmic losses in the geodynamo.

The arrows between the kinetic and magnetic energies in Fig. 1 indicate that energy can flow in either direction. While a net transfer of energy from kinetic to magnetic is needed to maintain the magnetic field, there can be persistent transfers of energy from magnetic to kinetic. Dynamic processes that draw energy from the magnetic field play an important role in equilibrating the magnetic field. For example, magnetic instabilities may limit the growth of the field by converting magnetic energy into kinetic energy. Alternatively, strong Lorentz forces can restrict the conversion of kinetic energy into magnetic energy. Both of these processes are evident in the energetics of the geodynamo model.

3 SPECTRAL DECOMPOSITION

Decomposition of the kinetic and magnetic energy equations into spectral components reveals how energy is converted from one form to another at different spatial scales. A spectral decomposition of the energy equations in (5) and (6) is also the only practical way of handling hyperdiffusion. We evaluate the spectral components of $\mathbf{v}$ and $\mathbf{B}$ using expansions in vector spherical harmonics.

The expansion for **B** takes the form

$$\mathbf{B} = \sum_{m=0}^{M} \sum_{l=1}^{L} \left(\mathbf{B}_{lm}^{P} + \mathbf{B}_{lm}^{T} \right) + \text{c.c.} \tag{13}$$

where superscripts P and T denote the poloidal and toroidal parts of the vector field at degree l and order m. Truncation of the expansion is imposed at $l = L$ and $m = M$ and we use c.c. to indicate the complex conjugate. The poloidal and toroidal components of the expansion are defined by

$$\mathbf{B}_{lm}^{P} = \nabla \times \nabla \times [b_{lm}(r, t) Y_{lm}(\theta, \phi) \hat{\mathbf{r}}] \tag{14}$$

$$\mathbf{B}_{lm}^{T} = \nabla \times [j_{lm}(r, t) Y_{lm}(\theta, \phi) \hat{\mathbf{r}}] \tag{15}$$

where $Y_{lm}(\theta, \phi)$ are the orthonormal spherical harmonic functions and the coefficients $b_{lm}(r, t)$ and $j_{lm}(r, t)$ describe the radial and temporal dependence of these fields. The expansion for **v** has identical form, where the coefficients of $\mathbf{v}_{lm}^{P}$ and $\mathbf{v}_{lm}^{T}$ are $v_{lm}(r, t)$ and $\omega_{lm}(r, t)$, respectively.

Vector spherical harmonics satisfy orthogonality relations (e.g. Chandrasekhar 1961), which allow the total magnetic and kinetic energies to be written as

$$\int_{V} \frac{\mathbf{B}^2}{2} \, dV = \sum_{m} \sum_{l} \left(\int_{V} \left| \mathbf{B}_{lm}^{P} \right|^2 + \left| \mathbf{B}_{lm}^{T} \right|^2 \, dV \right) \tag{16}$$

$$\int_{V} \frac{Ro\mathbf{v}^2}{2} \, dV = \sum_{m} \sum_{l} \left(Ro \int_{V} \left| \mathbf{v}_{lm}^{P} \right|^2 + \left| \mathbf{v}_{lm}^{T} \right|^2 \, dV \right) \tag{17}$$

where $|\ |$ indicates the absolute value. Because each vector harmonic in the expansion of **B** and **v** makes an independent contribution to the total magnetic and kinetic energies, we can derive energy equations for each component of the magnetic and kinetic energy in (16) and (17). Using the definitions given in (14) and (15), the toroidal and poloidal parts of the magnetic energy may be expressed in terms of the scalar coefficients b_{lm} and j_{lm} as

$$\int_{V} \left| \mathbf{B}_{lm}^{T} \right|^2 \, dV = l(l + 1) \int_{r_i}^{r_o} |j_{lm}|^2 \, dr \tag{18}$$

$$\int_{V} \left| \mathbf{B}_{lm}^{P} \right|^2 \, dV = l(l + 1) \int_{r_i}^{r_o} \frac{l(l + 1)}{r^2} |b_{lm}|^2 + |\partial_r b_{lm}|^2 \, dr \tag{19}$$

where r_i is the inner radius of the shell and ∂_r denotes differentiation with respect to r. Analogous expressions for the toroidal and poloidal parts of the kinetic energy at l and m are written in terms of the coefficients ω_{lm} and v_{lm} (see Appendix).

The spectral form of the energy equations are obtained by differentiating (18) and (19) (and their counterparts for kinetic energy) with respect to time. Consider the evolution of the toroidal magnetic energy,

$$\frac{\partial}{\partial t} \int_{V} \left| \mathbf{B}_{lm}^{T} \right|^2 \, dV = l(l + 1) \int_{r_i}^{r_o} j_{lm}^{*} \partial_t j_{lm} \, dr + \text{c.c.}, \tag{20}$$

where ∂_t denotes differentiation with respect to time and $*$ indicates the complex conjugate. An expression for $\partial_t j_{lm}$ is derived from the magnetic induction equation (e.g. Kuang & Bloxham 1999):

$$\partial_t j_{lm} = -H_{\eta}(l) D_l j_{lm} + \frac{r^2}{l(l + 1)} f_{lm}^{(1)} \tag{21}$$

where the operator D_l is defined by

$$D_l = \left(\frac{l(l + 1)}{r^2} - \partial_r^2 \right) \tag{22}$$

and

$$f^{(1)} = \hat{\mathbf{r}} \cdot \nabla \times \nabla \times (\mathbf{v} \times \mathbf{B}). \tag{23}$$

Using (21) in (20) yields

$$\frac{\partial}{\partial t} \int_{V} \left| \mathbf{B}_{lm}^{T} \right|^2 \, dV = -l(l + 1) H_{\eta}(l) \int_{r_i}^{r_o} j_{lm}^{*} D_l j_{lm} \, dr$$
$$+ \int_{r_i}^{r_o} r^2 j_{lm}^{*} f_{lm}^{(1)} \, dr + \text{c.c.}. \tag{24}$$

The first term on the right-hand side of (24) represents the ohmic losses (including the losses that occur inside the inner core and conducting part of the mantle) and the second term describes the generation of magnetic energy due to fluid motion (see Appendix A for details). The procedure outlined here uses the spectral equations from the geodynamo model to ensure consistency with the energy equations.

The equations for the poloidal part of the magnetic energy and the components of the kinetic energy are derived in a completely analogous fashion. We defer the derivation to Appendix A and give below only the equation for the toroidal part of the kinetic energy in order to identify several key points that are specific to the kinetic energy equations. The rate of change of the toroidal kinetic energy is given by

$$Ro \frac{\partial}{\partial t} \int_{V} \left| \mathbf{v}_{lm}^{T} \right|^2 \, dV = -l(l + 1) H_{v}(l) \int_{r_i}^{r_o} E \omega_{lm}^{*} D_l \omega_{lm} \, dr$$
$$+ \int_{r_i}^{r_o} r^2 \omega_{lm}^{*} f_{lm}^{(3)} \, dr$$
$$+ \int_{r_i}^{r_o} r^2 \omega_{lm}^{*} f_{lm}^{(4)} \, dr + \text{c.c.}, \tag{25}$$

where $f^{(3)} = \hat{\mathbf{r}} \cdot \nabla \times (\mathbf{J} \times \mathbf{B})$ and $f^{(4)} = \hat{\mathbf{r}} \cdot \nabla \times (\hat{\mathbf{z}} \times \mathbf{v})$. The first term on the right-hand side of (25) represents the viscous dissipation, while the second term quantifies the work done by the Lorentz force. The third integral involves the Coriolis force, which is written in non-dimensional form as $\hat{\mathbf{z}} \times \mathbf{v}$. Because $\hat{\mathbf{z}} \times \mathbf{v}$ is orthogonal to **v**, the Coriolis force does no work. However, the Coriolis force can redistribute kinetic energy across the vector harmonic components of **v** without making a net contribution. We have chosen to eliminate the effects of the Coriolis force by summing over the spectral components of the kinetic energy that are coupled by $\hat{\mathbf{z}} \times \mathbf{v}$. The nature of this coupling is revealed by expanding $f^{(4)}$ in spherical harmonics. Coefficients $f_{lm}^{(4)}$ in (25) depend on the velocity scalars ω_{lm} and $v_{(l \pm 1)m}$ (e.g. Kuang & Bloxham 1999), which means that spectral components with common m and adjacent l are coupled together. An analogous expansion of the Coriolis force in the poloidal equation yields a similar dependence between v_{lm} and $\omega_{(l \pm 1)m}$. We eliminate the effects of coupling due to the Coriolis force by summing $|\mathbf{v}_{lm}^{T}|^2$ and $|\mathbf{v}_{lm}^{P}|^2$ over l for a given value of m. The resulting spectrum of kinetic energy is then presented as a function of m. We denote the components of this spectrum by $Ro|\mathbf{v}_m|^2$, and obtain the total kinetic energy by summing over m. The magnetic energy spectrum $|\mathbf{B}_m|^2$ is also presented as a function of m.

Part of our motivation for presenting the spectra as a function of m is due to the columnar structure of convection (e.g. Olson & Glatzmaier 1995). Spherical harmonic components of the velocity must be summed over l to construct the columnar pattern of flow observed in the geodynamo model. We are also motivated by the fact that transfers of energy between m are due solely to the nonlinear terms in the governing equations. These terms include the

magnetic source term in the induction equation and the Lorentz force in the momentum equation, which are collectively responsible for transfers of energy between kinetic and magnetic forms (see Fig. 1). We gain useful insights into the nature of these transfers when the spectra are presented as functions of m. However, there are several disadvantages with our approach. First, derivatives in the spectral equations (such as D_l in eq. 22) depend on l rather than m, so it is more natural to define a horizontal length scale in terms of l. Second, the effects of hyperdiffusion are represented as functions of l, which means that our spectra of ohmic and viscous dissipation include spectral components with a range of values for the magnetic diffusivity and viscosity. We address these problems in the next section, where we present specific results from the Kuang–Bloxham model.

4 TEMPORAL AND SPATIAL VARIATIONS

Time-averaged spectra from a representative calculation of Kuang & Bloxham (1999) are shown in Fig. 2 (Table 1 lists the parameter values used in the simulation). We present spectra for the kinetic and magnetic energies, as well as the viscous and ohmic dissipation. The kinetic and magnetic energy spectra are comparable in magnitude and overall shape. Both spectra have large $m = 0$ terms which reflect a large zonal circulation and a strong zonal (toroidal) magnetic field.
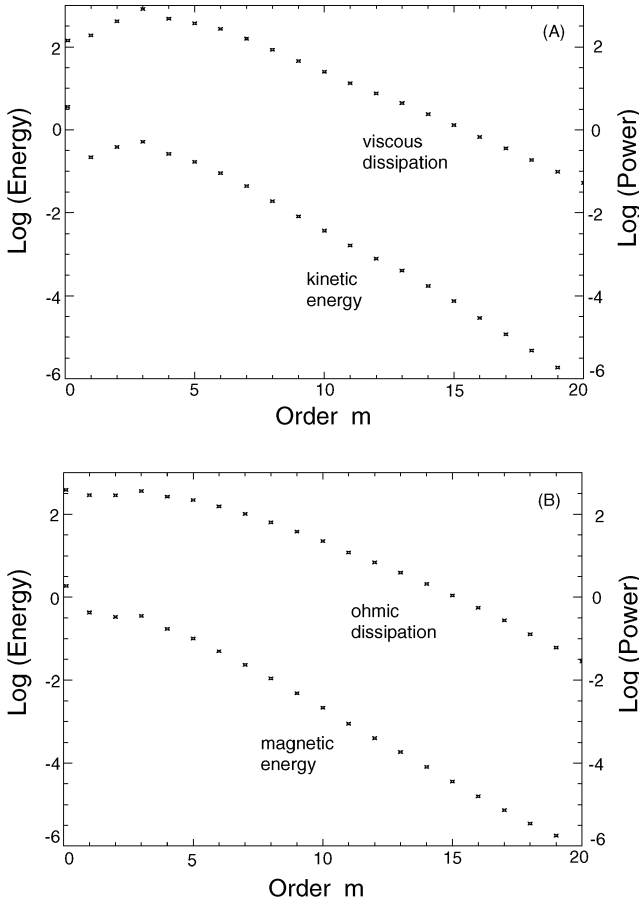
Figure 2. Time-averaged spectra of (a) kinetic energy and viscous dissipation, and (b) magnetic energy and ohmic dissipation as a function of angular order m. Both the energy and power are expressed in dimensionless form (see text for definitions).

Table 1. Dimensionless parameters.

Parameter	Symbol	Value
Rossby number	Ro	2×10^{-5}
Ekman number	E	2×10^{-5}
Rayleigh number	Ra	1.5×10^{4}
Hyperviscosity	H_ν	$1 + 0.05l^2$
Hyperdiffusion	H_η	$1 + 0.06l^2$

The higher order components are smaller and vary systematically with changes in m. The rates of decay of the two energy spectra are nearly equal once m exceeds $m = 5$.

The dissipation spectra follow the trends of the energy spectra in Figs 2(a) and (b). More quantitative comparisons of the energy and the dissipation yield estimates for the characteristic length scale L_m of the velocity and magnetic fields at each m. An order of magnitude estimate for the viscous dissipation is given by

$$\Phi_m^\nu = \frac{\nu_m |\mathbf{v}_m|^2}{L_m^2} \tag{26}$$

where $|\mathbf{v}_m|^2$ is inferred from the time-averaged kinetic energy and ν_m is the effective viscosity at order m. Similarly, the ohmic dissipation is approximated by

$$\Phi_m^\eta = \frac{\eta_m |\mathbf{B}_m|^2}{L_m^2} \tag{27}$$

where $|\mathbf{B}_m|^2$ is the time-averaged magnetic energy and η_m is the effective diffusivity. Estimates of L_m may be recovered from either (26) and (27) using the time-averaged dissipation spectra for Φ_m^ν and Φ_m^η. The effects of hyperdiffusion are included in ν_m and η_m by defining an average l for each value of m in the spectra. One possible definition is based on the distribution of kinetic energy over l at each m. Letting $|\mathbf{v}_{lm}|^2$ be the components of the kinetic energy that contribute to $|\mathbf{v}_m|^2$, we define

$$\bar{l}_1(m) = \sum_{l=m}^{L} \frac{l|\mathbf{v}_{lm}|^2}{|\mathbf{v}_m|^2} \tag{28}$$

and evaluate the effective diffusivities using $\eta_m = \eta H_\eta(\bar{l}_1)$ and $\nu_m = \nu H_\nu(\bar{l}_1)$. There are no significant differences if $\bar{l}_1$ defined in terms of the magnetic energy instead of the kinetic energy because the distributions of these two energies are very similar. However, other definitions are possible, so we consider a second average $\bar{l}_2$ in which the weighting is based on the spectral components of the ohmic dissipation instead of the kinetic energy. In Fig. 3, we compare the dissipation length scales L_m obtained using $\nu_m = \nu H_\nu(\bar{l}_1)$ in (26) with the values obtained using $\eta_m = \eta H_\eta(\bar{l}_2)$ in (27). The differences are relatively small, especially when compared with the azimuthal $L_\phi = \bar{r}/m$, and the meridional $L_\theta = \bar{r}/\sqrt{\bar{l}_1(\bar{l}_1 + 1)}$ length scales at low m. The average radius in the two horizontal length scales is given by $\bar{r} = (r_0 + r_i)/2$.

We expect L_m to represent the shortest length scale of the motion because it characterizes the effects of dissipation. Horizontal length scales L_ϕ and L_θ are substantially longer than L_m at low m, which suggests that dissipation is controlled mainly by radial variations in the magnetic and velocity fields. Differences between L_m, L_θ and L_ϕ reflect the structure of convective flow. Braginsky & Meytlis (1990) have previously argued that large differences in length scales are expected in the Earth's core. Rotation produces longer length scales in the direction of the rotation axis, while a
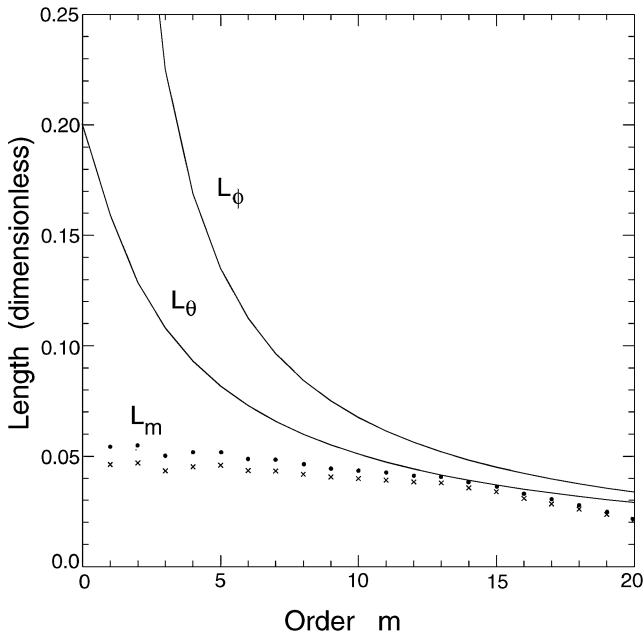
Figure 3. Dissipation length scale L_m recovered from a comparison of the kinetic (magnetic) energy and viscous (ohmic) dissipation spectra. Estimates for the average $\bar{l}$ are required to determine the effective diffusivity. Two different definitions for $\bar{l}$ yield two sets of values for L_m. The crosses gives the result for L_m obtained using $\bar{l}_1$ in (26), while the solid circles are obtained using $\bar{l}_2$ in (27). (See text for definition of $\bar{l}_1$ and $\bar{l}_2$.) Differences between these two definitions of L_m are small enough to neglect. The horizontal length scales are $L_\phi = \bar{r}/m$ and $L_\theta = \bar{r}/\sqrt{\bar{l}_1(\bar{l}_1+1)}$, where $\bar{r} = (r_o + r_i)/2$, are shown for comparison.

strong toroidal field can result in longer length scales in an azimuthal direction. The shorter length scale typically develops in the perpendicular direction, which corresponds to the radial direction in cylindrical coordinates, according to the analysis of Braginsky & Meytlis (1990). Outside of the polar regions of the core, we expect the long length scales in the axial and azimuthal directions to be manifest as large L_θ and L_ϕ. Thus the perpendicular direction corresponds to the radial direction in spherical geometries over a large volume of the core. The nearly constant value of L_m in Fig. 3 means that convection is most anisotropic at the largest scales, where the effects of viscosity are weakest. Some of the anisotropy inferred from Fig. 3 may also be attributed to the effects of hyperdiffusion because current implementations apply the enhanced damping to horizontal variations only (Grote *et al.* 2000b). Convergence of L_m, L_θ and L_ϕ at large m suggests that any contribution from hyperdiffusion is small once m becomes large. By comparison, we expect rotation and the magnetic field to have less influence on the structure of convection at large m as the viscous force becomes comparable to Coriolis and Lorentz forces, so the structure of convection inferred from Fig. 3 is compatible with the analysis of Braginsky & Meytlis (1990).

The combined effects of viscous and ohmic dissipation are compared with the gravitational energy release in Fig. 4. The time-averaged components of the gravitational energy release are plotted with positive values because they contribute to the kinetic energy at each m, whereas the viscous and ohmic dissipation represent energy sinks. The total dissipation spectrum mirrors the release of gravitational energy at all m. The peak in the spectra at $m = 3$ coincides with the dominant pattern of convective in the core. Fig. 5 shows
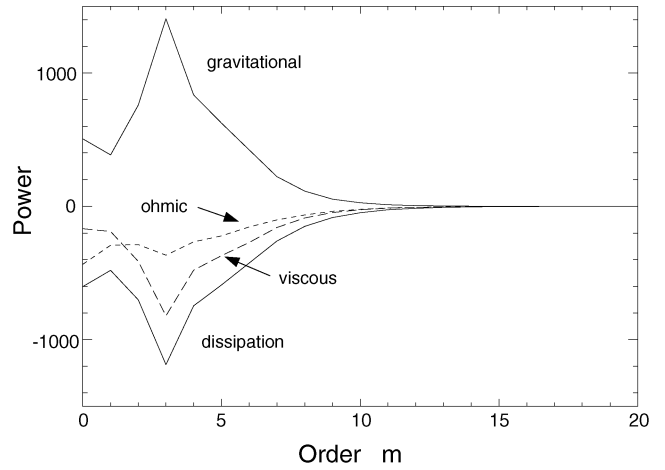

Figure 4. Time-averaged spectra of the gravitational energy release and the dissipation (viscous and ohmic) as a function of angular order m. The peak in the gravitational energy spectrum corresponds to the dominant pattern of convection in the geodynamo model.

two snapshots of flow through the surface $z = 0.4r_o$, which is parallel to the equator and slightly above the inner core ($r_i = 0.35r_o$). Red indicates the motion of warm fluid rising in columns that align with the rotation axis, while blue indicates the motion of cold, dense fluid. For the time step shown in Fig. 5(a), the dominant pattern of flow occurs at $m = 2$ and 3, whereas the dominant pattern at a later time step (Fig. 5b) is characterized by $m = 5$. Visual indications of the dominant pattern of flow are reflected quantitatively in the release of gravitational energy at these two time steps. When the spectra are averaged over time, a sharp peak emerges at $m = 3$.

To a first approximation, the time-averaged release of gravitational energy at each m is balanced by the combined effects of viscous and ohmic dissipation at the same spatial scale. We also find that the gravitational energy release balances the viscous and ohmic losses at each instant in time. Fig. 6 shows the temporal variability of the gravitational energy release and the separate contributions of ohmic and viscous dissipation (plotted again as negative values). The combined losses due to ohmic and viscous dissipation differ in absolute value from the rate of gravitational energy release by less than 10 per cent at most time steps. The significance of this temporal balance may be assessed by adding the magnetic (5) and kinetic (6) energy equations. Because the generation of magnetic energy by induction is equal and opposite to the work done by Lorentz forces, the balance between gravitational energy release and dissipation implies that the rates of change of magnetic and kinetic energy in (5) and (6) are small. Indeed the root mean square (RMS) of the temporal variation in magnetic energy is about an order magnitude smaller than the ohmic losses. The RMS variation in the kinetic energy is even smaller, and most of this variation occurs in the large zonal component (see Fig. 2a). Strictly speaking, variations in the non-zonal kinetic energy are not included in the energy budget because the inertial term is dropped from the momentum equation in the Kuang and Bloxham model when solving for the non-zonal part of **v**. Only the inertia in the zonal flow is retained. Nevertheless, we can still use the solution to estimate the change in the non-zonal kinetic energy between time steps. The fact that it is negligible in the overall energy budget is then compatible with the approximation used in the model.
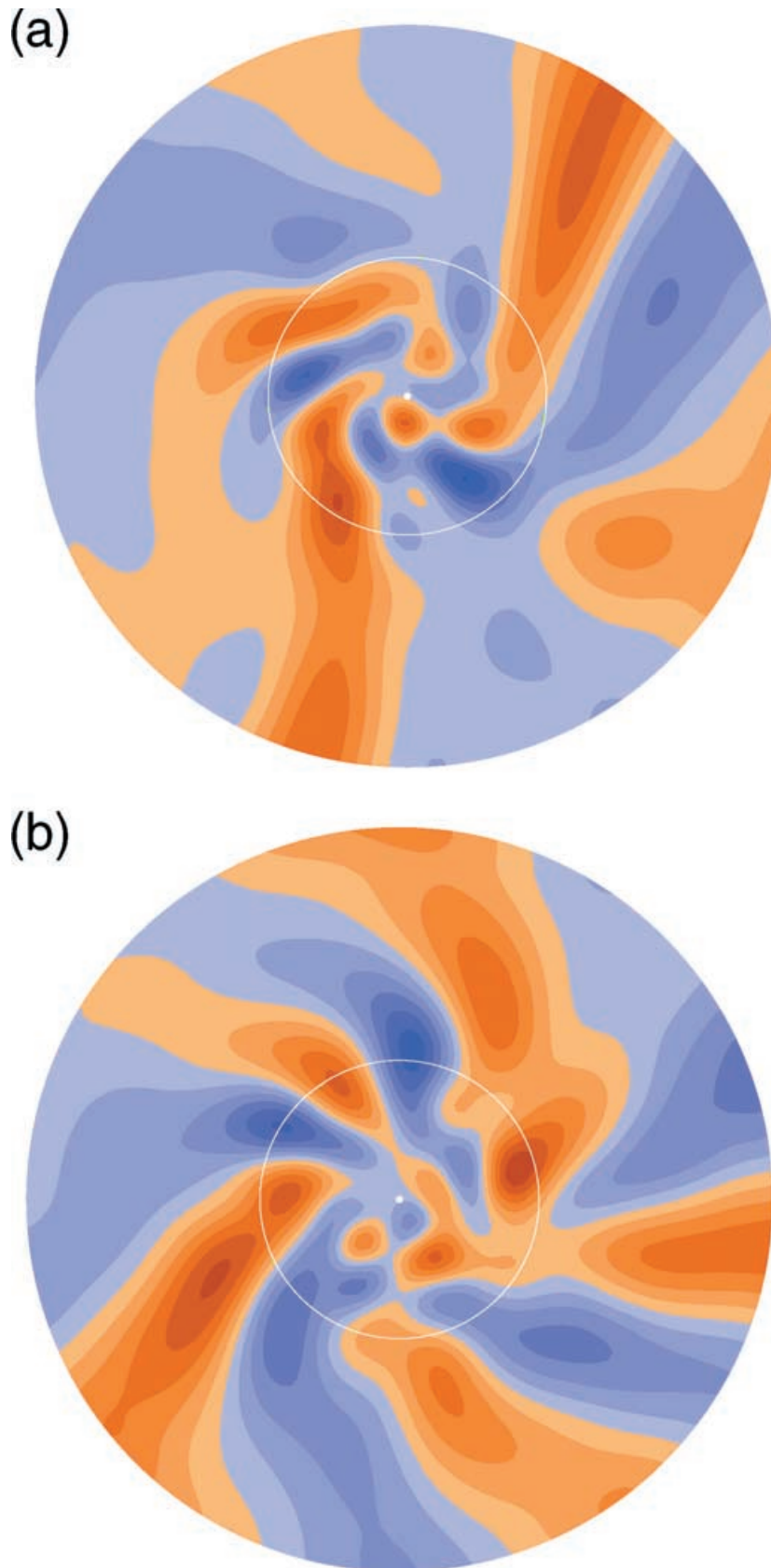
Figure 5. Snapshots of flow through the surface $z = 0.4r_o$, which is parallel to the equator and slightly above the inner core ($r_i = 0.35r_o$). Red corresponds to the flow of hot upwelling fluid, while blue corresponds to the flow of cold downwelling fluid. The dominant pattern of convection at the time step in (a) is associated with $m = 2$ and 3, while convection at a later time (b) has a strong $m = 5$ component. Time averages indicate that the dominant pattern of convection occurs at $m = 3$. The white circle indicates the outline of the inner core at the equator.
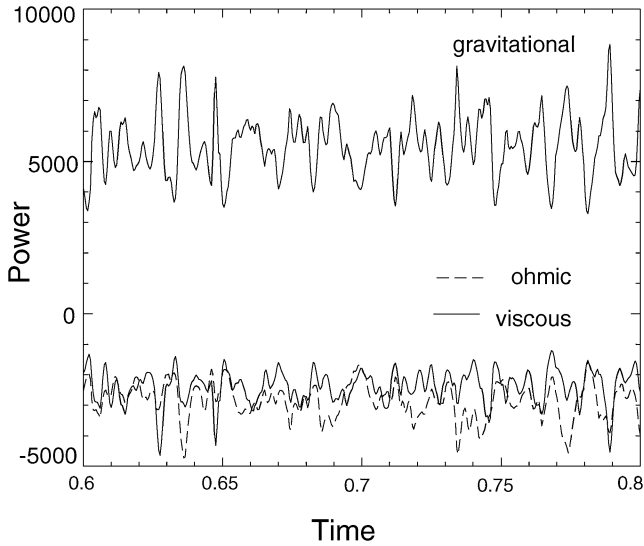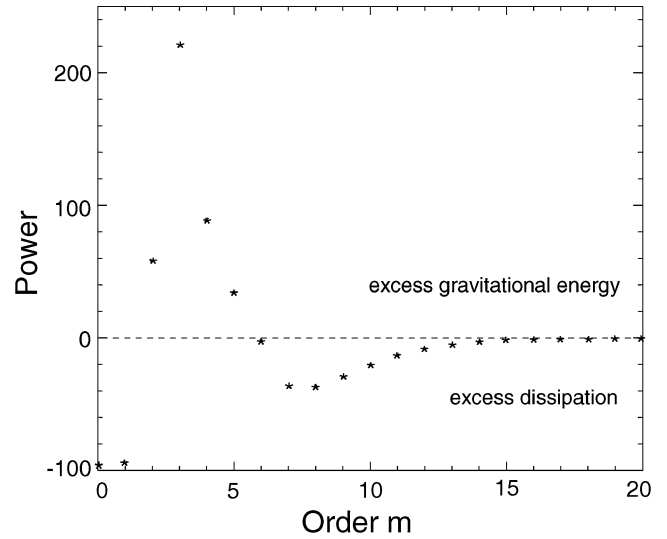
Figure 6. Temporal variation in the gravitational energy release and the dissipation. The viscous and ohmic dissipation are comparable in magnitude. The absolute value of the combined viscous and ohmic losses differs from the gravitational energy release by less than 10 per cent at most time steps.

Figure 7. Difference between the time-averaged gravitational energy release and the total dissipation as a function of m. Release of gravitational energy exceeds the dissipation between $m = 2$ to 5, whereas dissipation exceeds the gravitational energy release at lower and higher m.

Close temporal and spatial correlation of the energy sources and sinks implies a quasi-steady balance between buoyancy forces and the retarding influences of viscous and magnetic forces. This leading-order description of the dynamics is realized when buoyant parcels of fluid rise slowly through a zonal magnetic field. From a spectral point of view, each m component of the density variation $\Delta\rho$ causes flow with the same order m when the (non-linear) inertial effects in the momentum equation are small. The resulting flow distorts the zonal magnetic field to produce a magnetic perturbation and ohmic losses with the same m. While this idealized process characterizes the energetics to a first approximation, it is unable to sustain the zonal magnetic field. We show in the next section that the energy required to sustain the axial dipole field (and hence the zonal toroidal field through the ω effect) is supplied primarily by fluid motion with $m \approx 5$. Indeed transfers of energy between scales (i.e. between m) are essential for the operation of the geodynamo.

Persistent transfers of energy between m are indicated by differences between the time-averaged spectra for gravitational energy release and dissipation (see Fig. 7). We find that the release of gravitational energy exceeds the dissipation between $m = 2$ to $m = 5$, whereas dissipation exceeds the gravitational energy release at lower and higher values of m. In order to sustain this imbalance in the time-averaged spectra, excess power from $m = 2$ to $m = 5$ must be continually transferred to larger and smaller scales. Energy is transferred to the dipole field ($m = 0$) by fluid motion at $m \approx 5$, whereas excess dissipation at $m > 5$ is maintained by a turbulent cascade of kinetic and magnetic energy. In the absence of strong inertial effects, the transfer of energy to small scales is driven by Lorentz forces and by induction effects that generate small-scale electric currents. We investigate the generation of the dipole field in the next section and quantify the turbulent transfers to small azimuthal scales in Section 6.

5   GENERATION OF THE DIPOLE FIELD

Fluid motion $\mathbf{v}$ generates magnetic energy through the induction term in (5). Spectral decomposition of the induction term indicates

how different parts of $\mathbf{v}$ and $\mathbf{B}$ regenerate the field. We are specifically interested in the spectral components of $\mathbf{v}$ and $\mathbf{B}$ that contribute to the axial dipole field. These terms are identified by exploiting the orthogonality of the vector spherical harmonics. We calculate the rate Γ at which energy is supplied to the axial dipole field using

$$\Gamma\left(\mathbf{B}_{10}^{P}\right) \equiv \int_{V} \left(\mathbf{B}_{10}^{P}\right)^{*} \cdot \nabla \times (\mathbf{v} \times \mathbf{B})\, dV + \text{c.c.} \qquad (29)$$

and apply well-known selection rules (Bullard & Gellman 1954) to evaluate the combinations of $\mathbf{v}$ and $\mathbf{B}$ that contribute to the poloidal ($l = 1$, $m = 0$) part of $\nabla \times (\mathbf{v} \times \mathbf{B})$. The relevant components of $\mathbf{v}$ and $\mathbf{B}$ share a common value of m, while the allowable values of l for either $\mathbf{v}$ or $\mathbf{B}$ have a restricted range. Summing the contributions from components of $\mathbf{v}$ and $\mathbf{B}$ with common m yields the spectral decomposition of $\Gamma(\mathbf{B}_{10}^{P})$ in Fig. 8. Time averages of $\Gamma(\mathbf{B}_{10}^{P})$ identify those components of the flow that consistently contribute to the axial
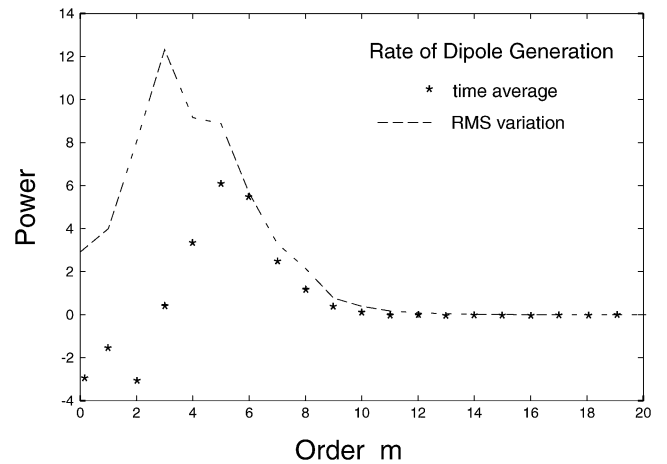
Figure 8. Power supplied to the dipole field as a function of the order m of the fluid motion. Points represent the time average and the dashed line indicates the RMS variation. The peak contribution to the dipole occurs at $m = 5$ and 6, while the largest RMS variation at $m = 3$ coincides with the peak in the gravitational energy release.

dipole, while the RMS variations indicate the amplitude of fluctuations caused by variations in the convective flow and by changes in the configuration of the magnetic field.

Fig. 8 reveals that positive contributions to the dipole field arise mainly from flow with $m = 5$ and 6. Positive contributions also arise from higher order components of flow, although the vigour of convection decreases at higher m, so these contributions are somewhat smaller. On the other hand, long wavelength components of flow ($m < 3$) draw energy away from the dipole field. In effect, the electric currents induced by flow at these scales must (on average) oppose the net electric current that maintains the dipole field. Thus the energy supplied to the axial dipole by induction includes persistent positive and negative contributions. The net rate at which energy is supplied to the dipole must (on average) equal the rate of ohmic decay. The RMS variations in the dipole generation are comparable to or larger than the time averages, so large fluctuations in the dipole amplitude are expected. Sustained intervals of smaller than average positive contributions from $m = 5$ and 6, combined with larger than average negative contributions at $m < 3$, drive down the dipole field, and may ultimately lead to a magnetic reversal. However, numerical calculations extending over many magnetic diffusion times show that large and sustained fluctuations in the dipole generation are relatively infrequent. At the present time, no magnetic reversals have occurred in the Kuang and Bloxham model using the parameter values listed in Table 1.

Simple expectations about the generation of the dipole field by helical flow in the outer core suggest that the dominant source of dipole field might arise from the dominant pattern of upwelling. However, comparison of the spectrum of gravitational energy release in Fig. 4 with the time-average dipole generation in Fig. 8 reveals that this is not the case. The dominant pattern of upwelling occurs at $m = 3$, whereas the peak contribution to the dipole occurs at $m = 5$ and 6. The largest RMS fluctuation in $\Gamma(\mathbf{B}_{10}^P)$ coincides with the dominant pattern of convection, but when $\Gamma(\mathbf{B}_{10}^P)$ is averaged over time the net contribution from flow at $m = 3$ nearly vanishes. This means that convection produces large inductive contributions to the dipole at $m = 3$, but these contributions are positive as often as they are negative. By contrast, flow at $m = 6$ makes a more consistent contribution to the dipole field in the sense that the time average is comparable to the RMS fluctuation. This suggests that fluid motions at different scales vary in their efficiency of dipole field generation. The scale dependence of dipole generation should be reflected in the local magnetic Reynolds number of the flow because this dimensionless number characterizes the relative importance of magnetic induction and diffusion. One definition of the local magnetic Reynolds number is given by

$$R_m = \frac{|\mathbf{v}_m|L_m}{\eta_m}, \qquad (30)$$

where $|\mathbf{v}_m|$ is inferred from the kinetic energy spectrum, L_m is the dissipation length scale defined by (27) and $\eta_m = \eta H_\eta(\bar{l}_1)$ is the effective diffusivity. The dissipation length scale represents the shortest length scale of the motion, so we would not expect R_m to be less than the value defined in (30). On the other hand, the representative length scale for dipole generation should not be greater than $L_\phi = r_o/m$, so an upper bound on R_m is obtained by replacing L_m with L_ϕ in (30). (Note that we now use r_o rather than $\bar{r}$ in the definition of L_ϕ.) These two definitions of R_m provide limiting values for evaluating the efficiency of dipole generation.

Our estimate for the efficiency of dipole generation accounts for differences in the vigour of convection by dividing the time-averaged value of $\Gamma(\mathbf{B}_{10}^P)$ at each m by the corresponding spectral component
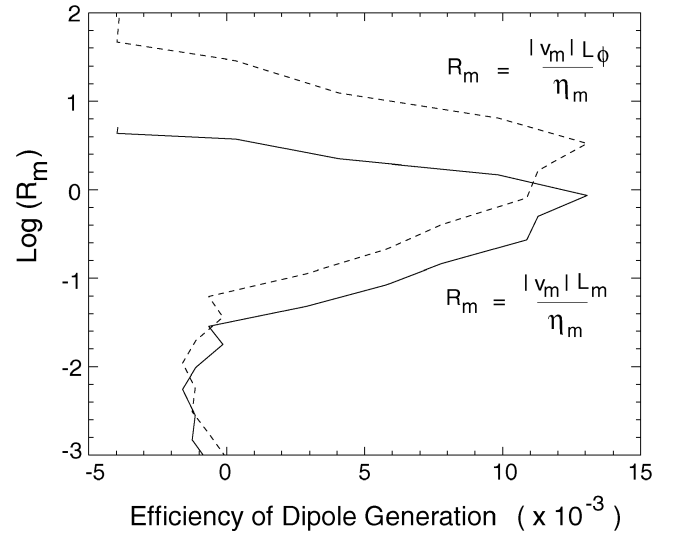

Figure 9. The efficiency of the dipole generation is defined by dividing the rate of energy supply $\Gamma(\mathbf{B}_{10}^P)$ by the rate of gravitational energy release at each m. It represents the fraction of the gravitational energy release which is diverted into the axial dipole field. The results are plotted as a function of the magnetic Reynolds number R_m. The definition of R_m in (30) gives a lower limit, while an upper limit is obtained by replacing L_m with L_ϕ. The peak efficiency in dipole generation occurs near $R_m \approx 1$.

of the gravitational energy release. The fraction of the gravitational energy release that is converted into magnetic energy in the axial dipole is plotted as a function of R_m in Fig. 9. We find that the efficiency of dipole generation is a sharply peaked function of R_m. The maximum occurs at $m = 6$, which corresponds to $R_m = 0.9$ or 3.3, depending on the definition of R_m. Components of flow with larger R_m (smaller m) make progressively smaller contributions to the dipole. Similarly, there is little contribution to the dipole from flow at shorter length scales once $R_m < 0.1$. Thus the flow that sustains the dipole field is confined to a relatively narrow range around $R_m \approx 1$.

We interpret this result by considering the influence of buoyant fluid rising through an initially zonal toroidal field (Parker 1955). Planetary rotation causes the rising fluid to lift and twist the toroidal field. If the local R_m of the upwelling is not too small, then a loop of magnetic field is added to the poloidal field. The associated electric current is directed perpendicular to the plane of the loop of field. Twisting the magnetic field to align the electric current with the mean zonal currents in the core reinforces the dipole field, whereas the opposite orientation reduces the dipole field. Our analysis of the geodynamo model indicates that a narrow range of R_m permits persistent constructive orientations of the magnetic field. When the local R_m is too small, the magnetic disturbance is insufficient to create a loop of field with the required orientation. However, when R_m is too large, the loop of field may be twisted through several revolutions, producing constructive and destructive orientations with equal likelihood. Continual regeneration of the dipole is attributed mainly to flow with local $R_m \approx 1$.

Mechanisms capable of sustaining the dipole field are collectively described as α-effects. The α-effect in the Kuang and Bloxham model is due mainly to the influence of upwelling and downwelling flow on the zonal toroidal magnetic field. This flow produces a magnetic perturbation with the same angular order m as the flow, and accounts for the close spectral correlation between the gravitational energy release and the dissipation in the model. Our characterization
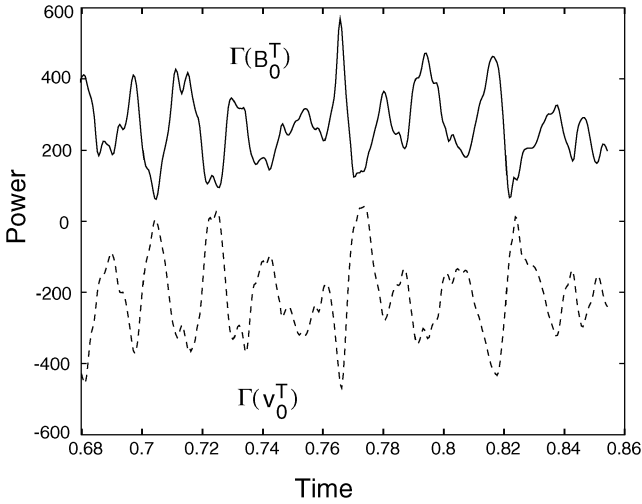
Figure 10. Temporal variations in the rate $\Gamma(\mathbf{B}_0^T)$ at which energy is supplied to the toroidal field and the rate $\Gamma(\mathbf{v}_0^T)$ at which energy is supplied to the toroidal circulation by Lorentz forces. The correlation of the two rates indicates the energy supplied to $|\mathbf{B}_0^T|^2$ is drawn from $Ro|\mathbf{v}_0^T|^2$. We infer that the toroidal magnetic field is generated mainly by the effects of shear in the zonal flow.

of the dynamo process is completed by describing the regeneration of the toroidal field. Decomposition of the magnetic energy equation indicates that the toroidal field is generated mainly from the dipole field by shear in the zonal circulation. This process is commonly referred to as the ω-effect.

Generation of the toroidal magnetic field at $m = 0$ is assessed by summing the rate at which energy is supplied to spherical harmonic components $\mathbf{B}_{l0}^T$. The source term for $\mathbf{B}_{l0}^T$ is calculated using

$$\Gamma\left(\mathbf{B}_{l0}^T\right) = \int_V \left(\mathbf{B}_{l0}^T\right)^* \cdot \nabla \times (\mathbf{v} \times \mathbf{B})\, dV + \text{c.c.} \tag{31}$$

and we sum $\Gamma(\mathbf{B}_{l0}^T)$ over l to obtain $\Gamma(\mathbf{B}_0^T)$. A typical result for $\Gamma(\mathbf{B}_0^T)$ as a function of time is shown in Fig. 10. The supply of magnetic energy to the toroidal field is consistently positive, although there are large fluctuations. The time dependence of $\Gamma(\mathbf{B}_0^T)$ is closely correlated with transfers of kinetic energy from the zonal flow by Lorentz forces. (We use the notation $\Gamma(\mathbf{v}_{lm}^T)$ to indicate the rate at which energy is supplied by Lorentz forces to the $\mathbf{v}_{lm}^T$ part of the flow.) We calculate $\Gamma(\mathbf{v}_{lm}^T)$ using

$$\Gamma\left(\mathbf{v}_{l0}^T\right) = \int_V \left(\mathbf{v}_{l0}^T\right)^* \cdot (\mathbf{J} \times \mathbf{B})\, dV + \text{c.c..} \tag{32}$$

and sum over l to obtain $\Gamma(\mathbf{v}_0^T)$. Comparison of $\Gamma(\mathbf{v}_0^T)$ and $\Gamma(\mathbf{B}_0^T)$ clearly shows that energy is transferred from the zonal flow into the toroidal field. The average change in kinetic energy is persistently negative and comparable to the average supply of energy to the toroidal field. Fluctuations in the energy transfers are closely coupled, leaving little doubt about the source of the energy for the toroidal field. Physically, shear in the zonal circulation distorts the dipole field (and smaller multipole components) to produce the zonal toroidal field. Electric currents associated with this zonal toroidal field produce Lorentz forces which slow the zonal circulation. This feedback on the zonal circulation equilibrates the generation of toroidal field. The process is sometimes called ω-quenching (Roberts & Soward 1992), and has long been used in mean-field dynamo models (e.g. Malkus & Proctor 1975; Proctor 1977). The interplay between the ω-effect and ω-quenching appears

to cause oscillations in the toroidal motion, which are not overly damped by viscous and ohmic losses.

6 ENERGY TRANSFER TO SMALL AZIMUTHAL SCALES

We have previously shown that the energy supplied by buoyancy-driven flow is balanced to a first approximation by dissipation at the same azimuthal scale (see Fig. 4). However, small imbalances are evident in the spectra (see Fig. 7). We find that dissipation exceeds the energy supplied by local convection once $m > 6$. The relative size of the imbalance actually increases systematically as m increases. At $m = 10$, for example, the combined effects of ohmic and viscous dissipation exceed the release of gravitational energy by a factor of 1.8. Once m increases to 15, the rate of energy loss exceeds the rate of energy supply by a factor of 2.8. These results indicate that the kinetic and magnetic energies at small azimuthal scales are too large to be explained by local convection. Instead, kinetic and magnetic energy must be transferred from small m to large m by non-linear interactions. In the absence of strong inertial effects, the transfer of energy to small azimuthal scales is driven by Lorentz forces $\mathbf{J} \times \mathbf{B}$ and by magnetic induction $\nabla \times (\mathbf{v} \times \mathbf{B})$.

The reader may question whether these energy transfers are important because even where the relative imbalance is large the overall magnitude is still quite small. Nevertheless, these energy transfers are precisely the phenomena that turbulent diffusivities are intended to represent. Realistic geodynamo models will inevitably require some type of representation for subgrid processes, so we are motivated to investigate these processes with the aim of improving the representations used in current geodynamo models.

Transfer of energy to small azimuthal scales can draw energy from either the large-scale velocity or magnetic fields. Indications of energy transfer from the large-scale velocity field were already evident in Fig. 10, where the source terms $\Gamma(\mathbf{B}_0^T)$ and $\Gamma(\mathbf{v}_0^T)$ are plotted as functions of time. Although $\Gamma(\mathbf{B}_0^T)$ and $\Gamma(\mathbf{v}_0^T)$ are highly correlated, small differences indicate that energy is not simply transferred from the zonal flow to the zonal magnetic field. For example, poloidal components of magnetic field with $m \neq 0$ are converted into toroidal components with the same m by shear in the zonal flow. As the toroidal component is amplified by the zonal flow, the combination of poloidal and toroidal components at order m produces a Lorentz force which opposes the shear in the zonal flow. Thus kinetic energy is transferred from the zonal flow into magnetic energy at order m. The source term $\Gamma(\mathbf{v}_0^T)$ in Fig. 10 includes all losses of kinetic energy from the zonal flow due to Lorentz forces. This includes the large Lorentz force that result from $\mathbf{J}$ and $\mathbf{B}$ with $m = 0$, as well as smaller contributions from fields with $m > 0$. The selection rules used in calculating $\Gamma(\mathbf{v}_0^T)$ require $\mathbf{J}$ and $\mathbf{B}$ to share a common value of m. Explicit decomposition of $\Gamma(\mathbf{v}_0^T)$ into spectral components in m quantifies how kinetic energy in the zonal flow is transferred into magnetic energy at different m. The transfer of (zonal) kinetic energy to magnetic energy at small azimuthal scales explains part of the excess magnetic energy inferred from Fig. 7. The remainder comes from kinetic energy in other parts of the flow.

Similarly, the source term $\Gamma(\mathbf{B}_0^T)$ is not restricted to the influence of zonal flow on the dipole field, although this is certainly the largest contribution. The selection rules used in calculating $\Gamma(\mathbf{B}_0^T)$ require $\mathbf{v}$ and $\mathbf{B}$ to share a common value of m. Once again, we can decompose the source term into spectral components according to this common value of m. Large, positive contributions to $\Gamma(\mathbf{B}_0^T)$ arise from the $m = 0$ part of $\mathbf{v}$ and $\mathbf{B}$. This reflects the influence of the zonal shear on the dipole field. However, smaller contributions also

arise from components of **v** and **B** with $m > 0$. In fact, all contributions from fields with $m > 0$ are persistently negative. This means that magnetic energy is drawn from the toroidal field at $m = 0$ and converted into kinetic energy at $m > 0$. Presumably, this transfer of energy to small azimuthal scales occurs through magnetic instabilities in the zonal field because the spectral components of $\Gamma(\mathbf{B}_0^T)$ can be correlated in time with increases in the corresponding spectral components of kinetic energy. However, the precise nature of these magnetic instabilities is not revealed using global energy balances. By decomposing $\Gamma(\mathbf{B}_0^T)$ into spectral components, we establish that losses of magnetic energy from $|\mathbf{B}_0^T|^2$ are transferred primarily into kinetic energy at $m = 2$, and that progressively smaller conversions into kinetic energy occur as m increases. The peak at $m = 2$ is at least compatible with the wavenumber of the most unstable modes in many stability calculations (e.g. Hutcheson & Fearn 1996; Fearn *et al.* 1997; McLean *et al.* 1999).

Part of the imbalance between the energy sources and sinks at small azimuthal scales is explained by transfers of kinetic and magnetic energy from $m = 0$. The remainder is attributed to small-scale Lorentz forces and electric currents that result from interactions between fields with $m > 0$. Quantifying these interactions provides insight into the turbulent cascade of energy. Of particular interest is the transport of energy to length scales below the resolution of the calculations. Currently, all geodynamo simulations use turbulent diffusivities to account for the influence of unresolved flow. Some simulations (Glatzmaier & Roberts 1995, 1996; Kuang & Bloxham 1997, 1999) use turbulent diffusivities that depend on the spherical harmonic degree l. Others adopt constant diffusivities (e.g. Christensen *et al.* 1998, 1999; Grote *et al.* 2000a). Questions about the use of scale-dependent diffusivities often focus on the introduction of spurious features in the predicted magnetic and velocity fields (Zhang & Jones 1997; Grote *et al.* 2000a). In identifying spurious features it is often tacitly assumed that constant diffusivities are preferable to scale-dependent diffusivities. However, this assumption cannot be justified when the influences of unresolved flow are not known. By adopting constant diffusivities we assume that interactions between the resolved and unresolved fields are independent of the length scale of the resolved fields. This assumption can be directly tested by quantifying the energy transfers between the long-wavelength ($m \leq 10$) and short-wavelength ($m > 10$) fields in the model of Kuang & Bloxham (1999). We confine our attention to the transfer of kinetic energy between long- and short-wavelength fields with the aim of describing the influence of short-wavelength fields in terms of a turbulent viscosity.

Estimates of turbulent viscosity reflect the transfer of kinetic energy by Lorentz forces because inertial effects are expected to be small in the Earth's core. This is also the case in the geodynamo model because the non-zonal inertial terms are not included in the momentum equation. We calculate the effect of the Lorentz force on the rate of change of kinetic energy in component $\mathbf{v}_{lm}$ using

$$\Gamma(\mathbf{v}_{lm}) = \int_V (\mathbf{v}_{lm})^* \cdot (\mathbf{J} \times \mathbf{B}) \, dV + \text{c.c.} \tag{33}$$

and sum over l to obtain $\Gamma(\mathbf{v}_m)$, which is the rate of change of kinetic energy in $\mathbf{v}_m$ due to the Lorentz force. Contributions to $\Gamma(\mathbf{v}_m)$ for components of flow with $m \leq 10$ can be divided into two parts. One part is calculated using components of **J** and **B** where both fields have $m \leq 10$. The second part includes components of **J** and **B** where either or both of these fields have $m > 10$. We are specifically interested in the second part because it would represent the influence of unresolved turbulence in a calculation truncated at $m = 10$.

We denote this part of $\Gamma(\mathbf{v}_m)$ by I_m and relate it to an effective viscosity.

Viscous stresses dissipate kinetic energy at a rate which depends on the viscosity ν_m of the fluid, the amplitude of the motion $|\mathbf{v}_m|$ and the characteristic length scale L_m. We have previously approximated the viscous dissipation by

$$\Phi_m^\nu = \frac{\nu_m |\mathbf{v}_m|^2}{L_m^2}, \tag{34}$$

where $\nu_m = \nu H_\nu(\bar{l}_1)$ is intended to represent the unmodelled influences of subgrid turbulence. Additional kinetic energy is lost from the long-wavelength motion as a result of Lorentz forces. The part of the energy loss associated with short-wavelength fields (namely I_m) can be characterized in terms of an effective turbulent viscosity $\tilde{\nu}_m$, which is defined by

$$I_m = \frac{\tilde{\nu}_m |\mathbf{v}_m|^2}{L_m^2}. \tag{35}$$

Estimates of $\tilde{\nu}_m$ are recovered from (35) using the kinetic energy spectrum to evaluate $|\mathbf{v}_m|^2$ and the dissipation length scale L_m from Fig. 3 (specifically the estimates indicated by crosses). The results in Fig. 11 are compared with the effective viscosity ν_m used in the geodynamo model.

Two conclusions may be drawn from Fig. 11. First, the effective viscosity ν_m, which is intended to represent the effects of turbulence in the geodynamo model, is substantially larger than the turbulent viscosity calculated explicitly using the short-wavelength fields. This means that fluid motions at long wavelengths (e.g. $m \leq 10$) are over damped in the calculation relative to the damping predicted by the effects of the (resolved) short-wavelength fields. Second, the turbulent viscosity is a strong function of m. The longest wavelengths are much less affected by turbulence than shorter wavelengths in
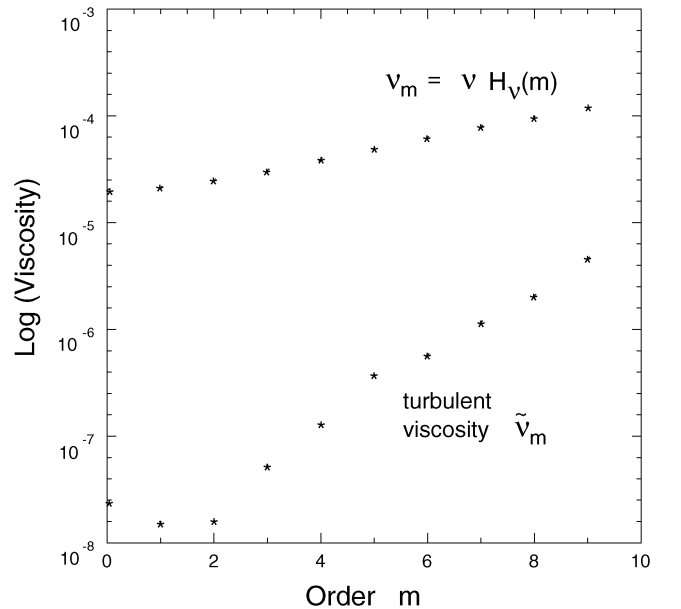
Figure 11. Estimates of the turbulent viscosity $\tilde{\nu}_m$ based on the transfer of kinetic energy from long wavelengths ($m \leq 10$) to short wavelengths ($m > 10$) in the geodynamo model. For comparison, we show the effective viscosity $\nu_m = \nu H_\nu(\bar{l}_1)$ used in the geodynamo calculations. The increase in ν_m with m is due to the use of hyperviscosity in the geodynamo model. A much larger rate of increase is evident in the turbulent viscosity $\tilde{\nu}_m$, indicating a strong dependence on wavenumber.

the range $m \leq 10$. Thus hyperviscosity appears to have some advantages from a purely energetic point of view because it lowers viscous damping at wavelengths where the effects of turbulent are less efficient. However, these energetic issues do not address whether hyperviscosity can be adequately represented by a simple function of spherical harmonic degree. Alternative strategies for including hyperviscosity may include replacing ∇^2 in the diffusion terms with higher-order operators, such as ∇^4 or ∇^6 (Dantinne *et al.* 1998; Busse 2000).

It is reasonable to ask whether the scale dependence of $\tilde{\nu}_m$ is a consequence of using hyperdiffusion in the geodynamo model. The counter point is whether strong scale dependence in $\tilde{\nu}_m$ can arise from relatively modest hyperdiffusion in ν_m. Definitive answers to these questions will have to await the analysis of numerical models that do not use hyperdiffusion. However, we can appeal to the global energy balance in Fig. 3 to speculate about the influence of hyperdiffusion on the energetics of the models. We expect hyperdiffusion to suppress the vigour of convection at small scales. This means that gravitational energy release and the associated ohmic and viscous dissipation decrease more rapidly with m when hyperdiffusion is included. Calculations with constant diffusivities would produce spectra of dissipation and energy (both kinetic and magnetic) that are flatter than those shown in Fig. 2. Increases in the relative amplitude of small-scale motion should enhance turbulent transport, but the structure of convection might not change substantially if the momentum equation continues to represent a simple balance between buoyancy forces and the retarding influence of viscous and magnetic forces. If we define local Ekman and magnetic Reynolds numbers from the numerical solution and relate their values to m, then we expect hyperdiffusion to alter the correspondence between the dimensionless numbers and m without fundamentally changing the operation of the geodynamo. Thus the inference of a strong scale dependence in $\tilde{\nu}$ should not be greatly affected by the use of hyperdiffusion in the geodynamo model.

7 CONCLUSIONS

We use global energy balances to analyse the geodynamo model of Kuang & Bloxham (1999). To a first approximation, we find that the gravitational energy released by buoyant fluid at angular order m is balanced by the combined effects of ohmic and viscous dissipation at the same m. Small imbalances between the spectral components of the gravitational energy release and the dissipation indicate that energy is transferred between azimuthal scales. Generation of the dipole field results mainly from fluid motion with $m = 5$ and 6. This part of the flow corresponds to a relatively narrow range of magnetic Reynolds number around $R_m \approx \mathcal{O}(1)$. Flow with larger values of R_m (smaller m) also contribute to the dipole field, but these contributions tend to cancel when averaged over time.

Transfer of energy to small azimuthal scales is the result of a turbulent cascade of kinetic and magnetic energy. Part of this energy is transferred from the large zonal fields, but the remainder is attributed to Lorentz forces and electric currents that result from interactions between fields with $m > 0$. We quantify the transfer of kinetic energy from large azimuthal scales ($m \leq 10$) to small azimuthal scales ($m > 10$) in terms of a turbulent viscosity. Estimates of the turbulent viscosity increase dramatically with decreasing length scale. This result supports the concept of hyperviscosity from an energetic point of view, although it does not indicate how hyperviscosity should be implemented in geodynamo models.

Comparison of the energy and dissipation spectra provides information about the structure of convection in the model. We find evidence for anisotropic flow with long length scales in the direction of the rotation axis and the strong toroidal field, as suggested previously by Braginsky & Meytlis (1990). Convection is most anisotropic at the largest wavelengths, where viscous forces are small compared with magnetic and Coriolis forces, although we cannot rule out a contribution from the anisotropic application of hyperdiffusion in the geodynamo model.

The methods we develop in this study provide global measures of the internal dynamics of geodynamo models. Time averages identify mean states, whereas temporal variations can establish causal connections between different physical processes. As an example we used the temporal variations in the generation of the toroidal magnetic field to show that the magnetic energy in this part of the field is supplied by converting kinetic energy from the zonal circulation. These tools are applicable to other geodynamo models and offer new diagnostics for assessing the operation of numerical models. More detailed comparisons of other geodynamo models will provide a better understanding of the consequences of underlying assumptions and help to identify new strategies for improving geodynamo models.

REFERENCES

Backus, G.E., 1975. Gross thermodynamics of heat engines in the deep interior of Earth, *Proc. Nat. Acad. Sci. USA,* **72,** 1555–1558.

Braginsky, S.I. & Meytlis, V.P., 1990. Local turbulence in the Earth's core, *Geophys. astrophys. Fluid. Dyn.,* **55,** 71–87.

Braginsky, S.I. & Roberts, P.H., 1995. Equations governing convection in Earth's core and the geodynamo, *Geophys. astrophys. Fluid. Dyn.,* **79,** 1–97.

Bullard, E.C. & Gellman, H., 1954. Homogeneous dynamos and terrestrial magnetism, *Phil. Trans. R. Soc. Lond.,* A., **247,** 213–278.

Busse, F.H., 2000. Homogeneous dynamos in planetary cores and in the laboratory, *Ann. Rev. Fluid Mech.,* **32,** 383–408.

Busse, F.H., Grote, E. & Tilgner, A., 1998. On convection driven dynamos in rotating spherical shells, *Stud. geophys. geod.,* **42,** 211–223.

Christensen, U., Olson, P. & Glatzmaier, G.A., 1998. A dynamo model interpretation of geomagnetic field structures, *Geophys. Res. Lett.,* **25,** 1565–1568.

Christensen, U., Olson, P. & Glatzmaier, G.A., 1999. Numerical modelling of the geodynamo: a systematic parameter study, *Geophys. J. Int.,* **138,** 393–409.

Dahlen, F.A & Tromp, J., 1998. *Theoretical Global Seismology,* Princeton University Press, Princeton, NJ.

Dantinne, G., Jeanmart, H., Winckelmans, G.S. & Legat, V., 1998. Hyperviscosity and vorticity-based methods for subgrid scale modeling, *Appl. Sci. Res.,* **59,** 409–420.

Fearn, D.R., Lamb, C.J., McLean, D.R. & Ogden, R.R., 1997. The influence of differential rotation on magnetic instability and nonlinear magnetic instability in the magnetostrophic limit, *Geophys. astrophys. Fluid. Dyn.,* **86,** 173–200.

Glatzmaier, G.A. & Roberts, P.H., 1995. A three-dimensional convective dynamo solution with rotating and finitely conducting inner core and mantle, *Phys. Earth planet. Inter.,* **91,** 63–75.

Glatzmaier, G.A. & Roberts, P.H., 1996. An anelastic evolutionary geodynamo simulation driven by compositional and thermal convection, *Physica D,* **97,** 81–94.

Grote, E., Busse, F.H. & Tilgner, A., 2000a. Regular and chaotic spherical dynamos, *Phys. Earth planet. Inter.,* **117,** 259–272.

Grote, E., Busse, F.H. & Tilgner, A., 2000b. Effects of hyperdiffusion on dynamo simulations, *Geophys. Res. Lett.,* **27,** 2001–2004.

Hewitt, J.M., McKenzie, D.P. & Weiss, N.O., 1975. Dissipative heating in convective flows, *J. Fluid Mech.,* **68,** 721–738.

Hutcheson, K.A. & Fearn, D.R., 1996. The stability of toroidal magnetic fields with equatorial symmetry, *Phys. Earth planet. Inter.,* **97,** 43–54.

Jones, C.A., Longbottom, A.W. & Hollerbach, R., 1995. A self-consistent convection driven geodynamo model using a mean-field approximation, *Phys. Earth planet. Inter.,* **92,** 119–141.

Kageyama, A. & Sato, T., 1998. Generation mechanism of a dipole field by a magnetohydrodynamical dynamo, *Phys. Rev. E,* **55,** 4617–4626.

Kuang, W., 1999. Force balances and convective state in the Earth's core, *Phys. Earth planet. Inter.,* **116,** 65–79.

Kuang, W. & Bloxham, J., 1997. An Earth-like numerical dynamo model, *Nature,* **389,** 371–374.

Kuang, W. & Bloxham, J., 1999. Numerical modelling of magnetohydrodynamic convection in a rapidly rotating spherical shell: Weak and strong field dynamo action, *J. Comp. Phys.,* **153,** 51–81.

Landau, L.D. & Lifshitz, E.M., 1987. *Fluid Mechanics,* 2nd edn, Pergamon Press, New York.

Malkus, W.V.R. & Proctor, M.R.E., 1975. The macrodynamics of α-effect dynamos in rotating fluids, *J. Fluid Mech.,* **67,** 417–443.

McLean, D.R., Fearn, D.R. & Hollerbach, R., 1999. Magnetic stability under the magnetostrophic approximation, *Phys. Earth planet. Inter.,* **111,** 123–139.

Olson, P. & Glatzmaier, G.A., 1995. Magnetoconvection in a rotating spherical shell: structure of flow in the outer core, *Phys. Earth planet. Inter.,* **92,** 109–118.

Olson, P., Christensen, U. & Glatzmaier, G.A., 1999. Numerical modeling of the geodynamo: Mechanisms of field generation and equilibration, *J. geophys. Res.,* **104,** 10 383–10 404.

Parker, E.N., 1955. Hydromagnetic dynamo models, *Astrophys. J,* **122,** 293–314.

Proctor, M.R.E., 1977. Numerical solution of the non-linear α-effect dynamo equations, *J. Fluid Mech.,* **80,** 769–784.

Roberts, P.H. & Soward, A.M., 1992. Dynamo theory, *Ann Rev. Fluid Mech.,* **24,** 459–512.

Zhang, K. & Jones, C., 1997. The effect of hyperviscosity on geodynamo models, *Geophys. Res. Lett.,* **24,** 2869–2872.

APPENDIX A: SPECTRAL FORM OF THE ENERGY EQUATIONS

Consistency between the energy calculations and the geodynamo model is enforced when the form of the momentum and induction equations in the geodynamo model is identical to that used in the energy equations. Kuang and Bloxham (1999) obtain solutions to the momentum and induction equations in terms of the coefficients of the spherical harmonic expansions of **v** and **B**. The evolution equations for these coefficients are given explicitly in Kuang & Bloxham (1999). In this appendix we derive the energy equations directly from the evolution equations for these coefficients.

Our starting point is the definition of the kinetic and magnetic energy in terms of the scalar coefficients. The toroidal and poloidal parts of the magnetic energy were given in (18) and (19). Analogous expressions for the toroidal and poloidal parts of the kinetic energy in terms of ω_{lm} and v_{lm} are

$$\int_V Ro\left|\mathbf{v}_{lm}^T\right|^2 dV = Rol(l+1)\int_{r_i}^{r_o} |\omega_{lm}|^2 \, dr, \tag{A1}$$

$$\int_V Ro\left|\mathbf{v}_{lm}^P\right|^2 dV = Rol(l+1)\int_{r_i}^{r_o} \frac{l(l+1)}{r^2}|v_{lm}|^2 + |\partial_r v_{lm}|^2 \, dr. \tag{A2}$$

Time derivatives of these expressions give the required energy equations. However, before we can use the evolution equations from Kuang and Bloxham, we must rearrange the poloidal terms into a more convenient form. Beginning with the kinetic energy equation we integrate the second term in (A2) by parts to obtain

$$\int_V Ro\left|\mathbf{v}_{lm}^P\right|^2 dV = Rol(l+1)\int_{r_i}^{r_o} v_{lm}^* D_l v_{lm} \, dr$$
$$+ Rol(l+1)v_{lm}^*\partial_r v_{lm}\Big]_{r_i}^{r_o} \tag{A3}$$

where D_l is defined in (22) and the second term vanishes because v_{lm} vanishes at the boundaries of the liquid core. Thus the time derivatives of the toroidal and poloidal kinetic energy become

$$\frac{\partial}{\partial t}\int_V Ro\left|\mathbf{v}_{lm}^T\right|^2 dV = Rol(l+1)\int_{r_i}^{r_o} \omega_{lm}^*\partial_t\omega_{lm} \, dr + \text{c.c.} \tag{A4}$$

$$\frac{\partial}{\partial t}\int_V Ro\left|\mathbf{v}_{lm}^P\right|^2 dV = Rol(l+1)$$
$$\times \int_{r_i}^{r_o} \frac{l(l+1)}{r^2} v_{lm}^*\partial_t D_l v_{lm} \, dr + \text{c.c.} \tag{A5}$$

We now substitute for $\partial_t\omega_{lm}$ and $\partial_t D_l v_{lm}$ from Kuang & Bloxham (1999). The toroidal scalar ω_{lm} is governed by

$$Ro\partial_t\omega_{lm} = -EH_\nu D_l w_{lm} + \frac{r^2}{l(l+1)}f_{lm}^{(3)} - \frac{r^2}{l(l+1)}f_{lm}^{(4)} \tag{A6}$$

where

$$f^{(3)} = \hat{\mathbf{r}}\cdot\nabla\times(\mathbf{J}\times\mathbf{B}) \tag{A7}$$

and

$$f^{(4)} = \hat{\mathbf{r}}\cdot\nabla\times(\hat{\mathbf{z}}\times\mathbf{v}). \tag{A8}$$

The poloidal scalar v_{lm} is governed by

$$R_o\partial_t D_l v_{lm} = -EH_\nu D_l^2 v_{lm} + \frac{r^2}{l(l+1)}f_{lm}^{(5)} - \frac{r^2}{l(l+1)}f_{lm}^{(6)} + RaT_{lm}, \tag{A9}$$

where

$$f^{(5)} = \hat{\mathbf{r}}\cdot\nabla\times\nabla\times(\mathbf{J}\times\mathbf{B}), \tag{A10}$$

$$f^{(6)} = \hat{\mathbf{r}}\cdot\nabla\times\nabla\times(\hat{\mathbf{z}}\times\mathbf{v}), \tag{A11}$$

and the scalar T is related to the temperature perturbation Θ by $T = r\Theta$. Introducing (A6) and (A9) into (A4) and (A5) completes the derivation of the kinetic energy equations.

We conclude with the derivation of the equation for poloidal magnetic energy. (The toroidal part was developed in Section 3.) The poloidal magnetic energy was given in (19) as

$$\int_V \left|\mathbf{B}_{lm}^P\right|^2 dV = l(l+1)\int_{r_i}^{r_o} \frac{l(l+1)}{r^2}|b_{lm}|^2 + |\partial_r b_{lm}|^2 \, dr. \tag{A12}$$

Integrating the second term by parts gives

$$\int_V \left|\mathbf{B}_{lm}^P\right|^2 dV = l(l+1)\int_{r_i}^{r_o} b_{lm} D_l b_{lm}^* \, dr + l(l+1)b_{lm}\partial_r v_{lm}^*\Big]_{r_i}^{r_o} \tag{A13}$$

so the rate of change of poloidal magnetic energy becomes

$$\frac{\partial}{\partial t} \int_V \left| \mathbf{B}_{lm}^P \right|^2 dV = l(l+1) \int_{r_i}^{r_o} \partial_t b_{lm} D_l b_{lm}^* \, dr$$
$$+ l(l+1) \partial_t b_{lm} \partial_r b_{lm}^* \Big|_{r_i}^{r_o} + \text{c.c.} \qquad (A14)$$

The scalar equation for $\partial_t b_{lm}$ from Kuang & Bloxham (1999) is

$$\partial_t b_{lm} = -H_\eta D_l b_{lm} + \frac{r^2}{l(l+1)} f_{lm}^{(2)}, \qquad (A15)$$

where

$$f^{(2)} = \hat{\mathbf{r}} \cdot \nabla \times \nabla \times (\mathbf{v} \times \mathbf{B}). \qquad (A16)$$

Substituting (A15) in (A14) yields

$$\frac{\partial}{\partial t} \int_V \left| \mathbf{B}_{lm}^P \right|^2 dV = -H_\eta l(l+1) \int_{r_i}^{r_o} |D_l b_{lm}|^2 \, dr$$
$$- H_\eta l(l+1) \partial_r b_{lm}^* D_l b_{lm} \Big|_{r_i}^{r_o} + \int r^2 D_l b_{lm}^* f_{lm}^{(2)} \, dr$$
$$+ r^2 \partial_r b_{lm}^* f_{lm}^{(2)} \Big|_{r_i}^{r_o} + \text{c.c.} \qquad (A17)$$

The first term on the right-hand side represents the ohmic dissipation due to the poloidal field in the interior of the liquid core, while the second term is equal to the surface integral in (4). The next two terms represent the effects of magnetic induction. Calculation of the spectral components of $f^{(2)}$ is facilitated by converting the expansions of $\mathbf{v}$ and $\mathbf{B}$ into generalized spherical harmonics in order to make use of well-known expressions for the integral over the product of three spherical harmonics (e.g. Dahlen & Tromp 1998). The same approach is used for all of the other non-linear terms.

Finally, we note that the surface integral in (5) does not explicitly appear in (20) for the magnetic energy in the toroidal part of the field. It is straightforward to show that

$$\int_S H_\eta \mathbf{J} \times \mathbf{B} \cdot d\mathbf{S} = -H_\eta l(l+1) j_{lm}^* \partial_r j_{lm} \Big|_{r_i}^{r_o} + \text{c.c.} \qquad (A18)$$

and

$$\int_V H_\eta J^2 \, dV = 2 H_\eta l(l+1) \int_{r_i}^{r_o} \frac{l(l+1)}{r^2} |j_{lm}|^2 + |\partial_r j_{lm}|^2 \, dr \qquad (A19)$$

when $\mathbf{B}$ and $\mathbf{J}$ refer to a single harmonic component of the toroidal magnetic field. Integrating the second term of (A19) by parts and combining the result with (A18) yields

$$\int_V H_\eta J^2 \, dV + \int_S H_\eta \mathbf{J} \times \mathbf{B} \cdot d\mathbf{S} = \int_r H_\eta l(l+1) j_{lm}^* D_l j_{lm} \, dr + \text{c.c.} \qquad (A20)$$

The term on the right-hand side of (A20) appears in the magnetic energy equation in (24), where it was described as the ohmic dissipation, including the losses that occur inside the inner core and conducting part of the mantle.